Plasma Chem Plasma Process (2012) 32:17–33
DOI 10.1007/s11090-011-9330-3

ORIGINAL PAPER

Low Pressure Radio Frequency Ammonia Plasma Surface Modification on Poly(ethylene terephthalate) Films and Fibers: Effect of the Polymer Forming Process

M. Ö. Öteyaka · P. Chevallier · S. Turgeon · L. Robitaille · G. Laroche

Received: 13 July 2011 / Accepted: 20 October 2011 / Published online: 23 November 2011

Abstract We investigated the effect of a polyethylene terephthalate (PET) forming process on radiofrequency ammonia plasma surface-treated PET flat films and fibres obtained by melt blowing. Ammonia plasma treatment allowed for the incorporation of amino functionalities on both the film and fibre surfaces, with higher values observed at very short treatment times. This plasma treatment also induced polymer chain scissions which were observed as the formation of hydrophilic nodules that coalesced together and were loosely bound to the underlying polymeric materials. These plasma-induced surface damages were notably more important on the melt-blown PET fibres. Consequently, maximisation of the surface amino groups with minimal polymer chain breaking was achieved using very short plasma treatment times (typically 1 s). We also demonstrated that the polymer forming process must be taken into account when plasma modifications are to be performed on PET, as it may already lead to polymer chain breakings subsequently added to those induced in the plasma environment.

Keywords Fragmentation · Plasma modification · Polyethylene terephtalate · Stability · Surface morphology

M. Ö. Öteyaka · P. Chevallier · S. Turgeon · G. Laroche (✉)
Centre de Recherche du Centre Hospitalier Universitaire de Québec, Hôpital St-François d'Assise, Quebec City, QC, Canada
e-mail: Gaetan.Laroche@gmn.ulaval.ca

M. Ö. Öteyaka · P. Chevallier · S. Turgeon · G. Laroche
Laboratoire d'ingénierie de Surface, Centre de Recherche sur les Matériaux Avancés (CERMA), Département de Génie des Mines, de la Métallurgie et des Matériaux, Université Laval, Quebec City, QC G1V 0A6, Canada

L. Robitaille
Institut des Matériaux Industriels (IMI), Conseil National de Recherches du Canada, Boucherville J4B 6Y4, Canada

Introduction

Polyethylene terephthalate (PET) possesses many intrinsic properties, such as transparency, solvency, thermal, and crease resistance, good barrier properties, resistance to fatigue, and high tenacity as either film or fibre [1–3], and is thus widely used in various applications including packaging, electronics, decorative coatings, magnetic tapes, textiles, composite materials, and biomedical industry devices [1–4]. A significant challenge remains, however, with regard to its hydrophobic surface and resulting low surface energy which leads, for example, to poor adhesiveness between fillers and matrix in composite materials [5, 6], and to low adhesion of printing, dyeing, and other finishing processes on textile fibres [7, 8]. In low-diameter arterial prostheses, PET intrinsic surface properties are at the origin of the absence of neoendothelium formation which is known to be one cause of graft failure [9–11]. This explains why PET textile prostheses are not used for diameters of less than 8 mm [9, 10, 12, 13].

In order to improve the surface properties of PET, many techniques can be used, such as chemical, thermal, mechanical, electrical, and plasma treatments [1, 2]. Plasma treatment is a popular technique because it is a dry process (environmentally friendly) and allows for greater uniformity of the modified surface, hence it is widely used for industrial applications [2, 14]. Furthermore, plasma treatments enable the modification of the first atomic layers of the surface without changing the bulk properties of the material [2, 6, 8, 15, 16]. Moreover, depending on the plasma gaseous environments and experimental parameters, surface modification can be modulated to privilege etching (degradation of polymeric chains) or/and surface functionalisation [1, 2, 14, 15, 17–21]. For example, Inagaki et al. performed plasma surface modification experiments on PET using either O_2, H_2, N_2, Ar, or NH_3 and demonstrated that the etching rate was strongly dependent upon the gas used [1]. They also evidenced that O_2, H_2, N_2, and Ar plasma enabled to essentially modify CH_2 groups and phenyl rings rather than ester groups in the PET polymer chains, while the exact opposite behaviour was observed in a NH_3 plasma environment [1]. These observations are mainly explained by the fact that the nature and/or concentration of the activated species (ions, neutrals, radical, photons) [22] created in a plasma environment depends on the gas used to make the discharge. These activated species, in turn, drive the subsequent surface modification process.

Other research groups have demonstrated that the position of the sample in the plasma reactor also has an important influence on both the extent and the nature of the surface modification. For instance, radicals are the only species capable of reaching the material surface in remote mode (after-glow), while samples located directly within the plasma discharge are subjected to radicals, ions, or electrons [4, 15, 20, 23].

Finally, in the case of polyesters, the initial chemical structure of the polymer has been shown to be of paramount importance in the type of subsequent plasma surface modification, [15, 17] as aromatic polyesters appear to be capable of stabilising radicals formed on the polymeric chains following ester group scissions (thus enabling an efficient functionalisation), whereas aliphatic polyesters are etched when subjected to plasma treatments [15, 17].

To our knowledge, the influence of the PET forming process on the surface modification by plasma has never been investigated. We therefore sought to compare the effect of plasma treatments on the surface modification of PET fibres and PET films, with emphasis on ammonia plasma treatments that promote the formation of surface amino groups which are recognised as improving cell adhesion and, [24–26] more importantly, may potentially also be used for further biomolecule conjugation [27, 28]. To this end, we examined the

dependence between PET structure geometry and plasma treatment duration. Surface chemical composition following plasma treatment was therefore characterised using X-ray Photoelectron Spectroscopy (XPS), while the evolution of the surface topography of untreated and treated PET film and PET fibre surfaces was determined by Atomic Force Microscopy (AFM) analyses. Finally, the stability of the surface-modified treated fibres and films was assessed by means of an ageing protocol in water.

Materials and Methods

Materials and Sample Preparation

Pieces of PET films (0.1 mm thickness, biaxial oriented, cristallinity ~55%) were purchased from Goodfellow (Huntingdon, England) while PET fibre mats (0.1 mm thickness, cristallinity ~45%) were produced by means of the melt-blowing technique. The PET film crystallinity was selected to match as closely as possible that of the PET fibres since polymer crystallinity is known to influence the resulting plasma treated surface chemistry [29]. Briefly, this process consisted of extruding PET through a multi-hole die (230-hole grid, nominal diameter 300 μm). Extruded strands of PET were blown by hot air at very high speed through a narrow gap sideways of the die, which enabled fibre stretching at various levels depending on the flow rate of the molten polymer. The resulting nonwoven fibre veils were then used to fabricate the nonwoven structures by stacking several fibre veils onto a metallic plate. The plate was then inserted into an autoclave under controlled temperature to consolidate an optimum time [*patent pending*]. The resulting fibre network displayed a porosity of 80–90%, with average fibre diameters of 2–6 μm [30]. Pieces of PET from the films and the fibre network were cut (4 cm × 1.6 cm), were ultrasonically and successively cleaned for 10 min in acetone, deionised water, and methanol, and finally were dried under vacuum until use. 5-bromosalicylaldehyde with a level of purity of 98% was purchased from Sigma-Aldrich Corporation (Milwaukee, WI, USA).

Surface Modification

Plasma treatments were performed in the discharge of a previously described home-made cylindrical plasma reactor [31–33] with high purity ammonia gas (Matheson Tri-Gas Inc., Newark, CA, USA), at 15 W, 13.56 MHz, and 300 mTorr for 1, 5, 30, 60, 100, and 200 s. Due to the configuration of the plasma reactor, both the PET films and PET fibre network were rolled into a PTFE tube prior to plasma treatment. Each experiment was reproduced in triplicate.

A derivatisation technique was used to quantify the amine surface concentration by means of vapor-phase chemical derivatisation using 5-bromosalicylaldehyde, as previously described [31, 32]. Briefly, the derivatisation reactions were performed in a vapor phase at 85°C for 2 h in a sealed glass tube containing a 1 cm-thick bed of soda-lime glass beads to separate the reagent and the reactive surfaces. The surfaces were then outgassed under vacuum overnight prior to analysis.

Ageing tests were performed to assess the stability of the grafted amines and to monitor any possible surface reorganisation. The plasma-treated PET films and fibre mats were washed ultrasonically at room temperature for 5 min in deionised water (pH 6) and subsequently dried under vacuum overnight prior to further analyses.

Surface Characterisation

Static contact angle measurements were first performed on the PET samples by means of the VCA 2500 XE system (AST, Billerica, MA, USA). At least five drops of deionised water (3 μL) were deposited on different areas of the sample surfaces. The experiments were performed in triplicate for each plasma condition.

XPS was used to determine the surface chemical composition of the PET films and fibre networks with and without plasma treatment as well as all of the surfaces that underwent chemical derivatisation or/and ageing tests. XPS spectra were recorded by means of a PHI 5600-ci spectrometer (Physical Electronics, Eden Prairie, MN, USA). A standard monochromatic aluminium X-ray source (Al $K_\alpha = 1\ 486.6$ eV) at 300 W with a neutraliser recorded the survey spectra (1 200.0 eV), while the high-resolution spectra were obtained with a monochromatic magnesium X-ray source (1 253.6 eV) at 300 W with no charge neutralisation. Detection was performed at 45° with respect to the normal surface and the analysed area was 0.005 cm^2. Three survey and high-resolution spectra were obtained for each sample, and each experiment using different plasma conditions was performed in triplicate. The curve fitting procedure of the components underlying the C1s peaks was performed by means of a least-squares minimisation procedure using a Gaussian–Lorentzian function and a Shirley-type background.

Surface topography was investigated by AFM using the tapping mode of a Dimension™ 3100 Atomic Force Microscope (Veeco, Woodbury, NY, USA) with a Supersharpsilicon™ tip (NanoWorld Innovative Technologies, Neuchâtel, Switzerland, tip radius <2 nm). Images were taken with 512 × 512 data acquisition at a scan rate of 0.5 Hz at room temperature in air. The surface topography was evaluated for areas of 500 × 500 nm^2 using the Nanoscope program. Surface roughness was determined using the Root Mean Square (R_{rms}) roughness parameter. The image analyses, area measurement, and distribution of the polymer nodules were done using CLEMEX Vision software (Longueuil, QC, Canada).

Results and Discussion

Contact Angle Analyses

The extent of hydrophilicity of the plasma-treated PET films and fibres was investigated by contact angle measurement. Figure 1 shows the variation in the contact angle of the PET films and fibres for treatment times ranging from 0 to 200 s. The average initial contact angle value was 62° for the PET films and 138° for the PET fibres. This initial difference is mainly explained by a topographic effect induced by the interwoven fibres which provided a significantly greater roughness, compared to a flat surface. The presence of surface contaminants (see below) may also be partly responsible for this high contact angle value.

In addition to surface roughness, contact angle values depend on the species created on the surface during the plasma treatment. For example, adding new polar groups (functionalisation) is likely to lead to lower contact angles, whereas etching reactions (polymeric chain degradation) induces higher contact angle values. After 1 s of ammonia plasma modification, the contact angle of the PET films decreased to 40° and thereafter remained essentially constant (Fig. 1). Similarly, the plasma duration did not appear to influence the contact angle value of the PET fibres which decreased from 138° to 5° after plasma treatment, meaning that the fibres became hydrophilic and therefore highly wettable immediately following the lighting of the plasma. In both samples, the decreased

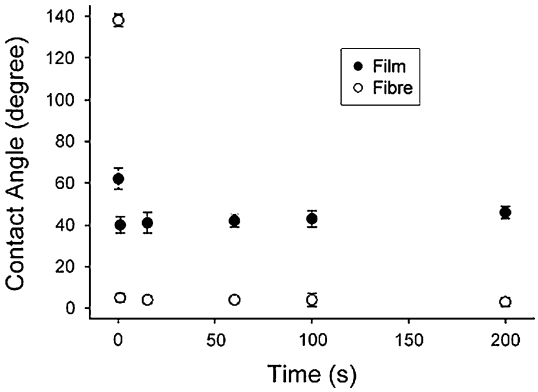

Fig. 1 Contact angle variation of the PET films and fibres as a function of plasma treatment time

contact angle recorded following plasma treatment was mainly due to the surface modification (polar group grafting) which could arise either from nitrogen-containing functionalities (most likely amino groups or oxygen surface species coming from residual oxygen/water present in the chamber). This was further investigated by surface chemical analyses.

Chemical Composition

XPS survey spectra enabled us to follow the surface chemical modifications through the atomic content variations. As can be seen in Fig. 2, the incorporation of nitrogen following the ammonia plasma treatment is clearly evidenced. The introduction of nitrogen-containing polar groups on the polymer surface may therefore be at the origin of the increased hydrophilicity obtained with the PET film.

Table 1 summarises the relative atomic surface carbon, nitrogen, and oxygen concentrations detected on the PET films and fibres before and after the plasma treatments. The

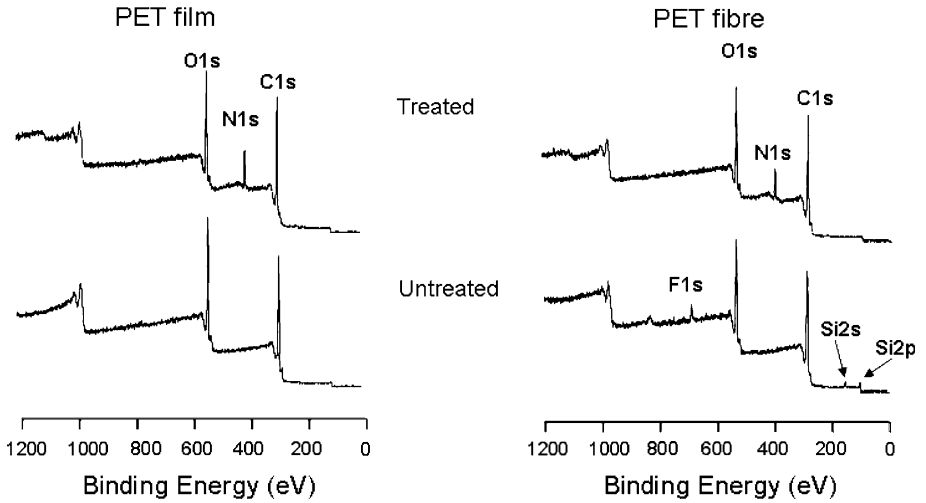

Fig. 2 Typical XPS survey spectra of the untreated and treated PET films and fibres after 200 s

Table 1 Chemical compositions from the XPS survey spectra of the untreated and ammonia plasma-treated PET films and fibres

Treatment time	FILM			FIBRE		
	O (%)	C (%)	N (%)	O (%)	C (%)	N (%)
Untreated[a]	28.9 ± 0.2	71.1 ± 0.2	–	26.1 ± 0.5	70.7 ± 0.9	–
Plasma 1 s	23.3 ± 0.9	67.2 ± 0.8	9.5 ± 0.5	22.7 ± 0.6	67.3 ± 0.7	10.0 ± 0.5
Plasma 15 s	23.1 ± 0.7	65.6 ± 0.9	11.3 ± 0.9	22.8 ± 0.5	64.3 ± 0.9	12.9 ± 0.8
Plasma 60 s	22.6 ± 0.7	66.3 ± 0.7	11.1 ± 0.4	21.8 ± 0.8	62.9 ± 0.7	15.3 ± 0.8
Plasma 100 s	22.9 ± 0.5	67.7 ± 0.8	9.4 ± 0.2	21.0 ± 0.3	60.5 ± 0.8	18.5 ± 0.9
Plasma 200 s	23.3 ± 0.9	65.5 ± 0.8	11.2 ± 0.5	19.9 ± 0.4	62.3 ± 0.7	17.8 ± 0.9

[a] The untreated PET fibre surfaces contained F (%) = 2.3 ± 0.9 and Si (%) = 0.9 ± 1.0

relative concentrations of C and O on the untreated films and fibres were expected, considering the chemical structure of PET (theoretical values: 71.4% C and 28.6% O). It should be noted that despite ultrasonic cleaning in different solvents, some contaminants (namely, fluorine and silicon) were detected on the untreated PET fibres, most likely due to contamination from the mat consolidation process. However, the XPS data showed that these elements were completely removed from the fibre surface upon plasma treatment.

The atomic surface concentrations of atoms detected by XPS on the plasma-treated PET films and fibres revealed that these polymer samples were successfully modified by the ammonia plasma, as approximately 10% of the nitrogen was introduced after only 1 s of treatment (Table 1). These surface concentration values did not appear to be dependent on the treatment time for the PET films, with the C, O, and N concentrations remaining almost steady for every plasma duration under study. In contrast, the N surface concentration on the PET fibres clearly increased with the plasma treatment duration, with values of 10.1% after 1 s up to approximately 18% after 200 s. Accordingly, the relative loss of carbon with respect to the untreated materials was 10% for the fibres and 6% for the films. For both types of surfaces, the oxygen surface concentration decreased by 5–6% regardless of the treatment duration. Because atomic surface concentrations measured through XPS provide only relative data, we calculated the surface atomic ratios (O/C, N/C) to acquire additional information on the effect of plasma treatments on PET samples (Fig. 3). For both surfaces under study, the plasma treatment duration led to an initial decrease of the O/C ratio from 0.4 to ~0.34 after 1 s, with no further significant modification between 5 and 200 s. The N/C ratio, on the other hand, differed for both surfaces. Indeed, this ratio slightly increased on the PET films after 1 s of treatment (from 0.15 to 0.18), with no significant subsequent variation up to 200 s, while that on the PET fibres, which also began at 0.15, continued to increase to attain a value of ~0.3 at 200 s of treatment.

Aside from the nitrogen surface incorporation, the selectivity of the grafting of nitrogen-containing species is of prime importance, as surface primary amino groups are the targeted species for further molecule conjugation. Plasma treatment selectivity is thus defined as the ratio of primary amino group surface concentration on that of all nitrogen-containing species (which include amines (NH_2), imines (C=NH), amides ($CO–NH_2$), and nitriles ($C \equiv N$), and is ascertained by means of a previously described surface derivatisation procedure [31]. Figure 3 presents the amine quantification results as well as the treatment selectivity. As shown in this figure, the highest amine concentrations were obtained following a plasma treatment of only 1 s for both the PET films and PET fibres, with 1.6 and

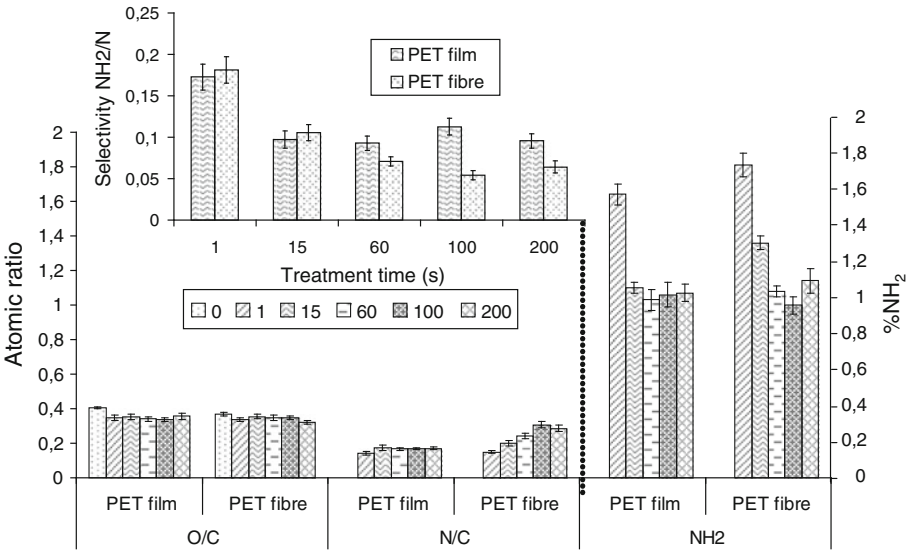

Fig. 3 Effect of treatment duration on chemical composition (O/C and N/C), amino concentration (NH_2), and selectivity (NH_2/N) of the treatment

1.8% of surface amino groups, respectively. Treatment performed for longer durations led to a decrease in the amino group surface content. Consequently, the most efficient plasma condition appeared to be a treatment of 1 s for both PET surfaces under study.

In order to further understand the nitrogen incorporation difference, High Resolution (HR) C1s XPS were recorded (Fig. 4). The binding energy of the core electrons surrounding carbon strongly depends on this atom's chemical environment and may thus provide valuable information regarding the nature of such surface modifications as N grafting, etching, unsaturation formation, aromatic ring scission, and decarboxylation. According to previously published data on plasma-treated PET, the peak located at 285.0 eV is caused by the polymer backbone aromatic ring and methyl side groups (C–C/C–H). Amine (C–N), ether, and alcohol groups (C–O) give rise to an XPS feature at 286.5 eV. Finally, XPS bands due to amide (NH_x–C=O) and nitrile (C≡N) are observable at 287.4 eV, while ester and carboxylic acid (O–C=O) are detectable at 289.0 eV. Of note is that the intensity of the $\pi - \pi^*$ shake–up band provides crucial data as to whether the aromatic ring remains intact upon plasma treatment. Table 2 describes the C1s XPS band evolution during the plasma process for the shorter and longer plasma treatment durations investigated.

First, the HR C1s XPS spectra of the untreated PET film (Table 2) perfectly matched the expected theoretical values for this polymer, with 60% of the carbon peak originating from the aromatic ring and the remaining 40% equally distributed between the C–O and O–C=O functionalities. In contrast, the HR C1s XPS spectra of the untreated fibres considerably differed from the expected results, with as much as 75% of the carbon being detected through the 285 eV feature and only 11.2% through the ester functionality (O–C=O at 289 eV). This difference cannot be explained solely by the presence of contaminants detected in the survey spectra, as the intensity of the $\pi - \pi^*$ shake-up band (291.4 eV), due to the aromaticity, was lower in the C1s spectra of the fibres than in those of the films (3.4% vs. 2.4%; Fig. 4). It may thus be assumed that the melt-blowing process used to make the fibre mats ultimately altered the PET chemical structure.

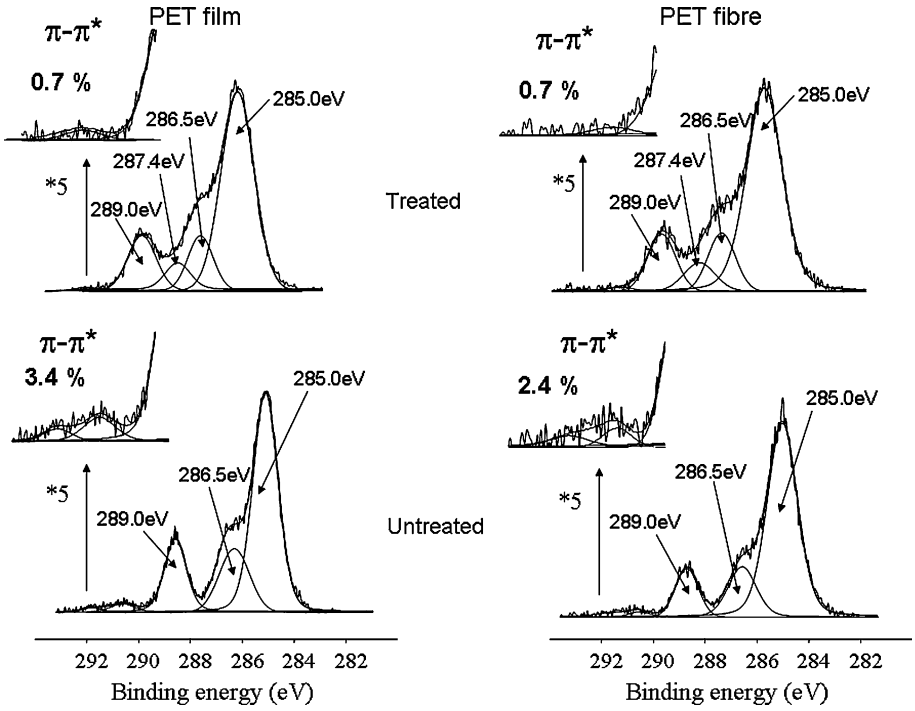

Fig. 4 HR C1s spectra of the untreated and plasma-treated PET films and fibres (plasma duration 200 s)

The HR C1s results clearly show that the plasma treatment on the PET films and fibres induced chemical changes (Table 2). The primary XPS spectrum modification was a new band at 287.4 eV attributed to amide groups and nitriles. This new band intensity did not appear to be dependent on the treatment time for either PET surface under investigation. In addition, the proportion of carbonyl band at 289 eV due to the initial ester group did not appear to be significantly affected by treatment time. Its broadening, however, as shown in Fig. 4, may be explained by the formation of carboxylic groups resulting from ester group scission during the plasma process. Indeed, Narushima et al. described various ester scission mechanisms in ammonia plasma leading either to carboxylic acid, amide, and amine group formation through the decarboxylation process [15]. Moreover, several authors clearly demonstrated that the aromatic ring is a key parameter in amine formation, as the benzene ring allows for the stabilisation of the radical that is formed following the decarboxylation process [1, 15–17]. However, these authors reported a decrease of the aromatic ring $\pi - \pi^*$ shake-up band, with no further explanations. In fact, Girardeaux et al. were the only group to suggest that the loss of intensity in the shake-up feature arose from a ring-opening phenomenon that occurred during the plasma treatment [20]. It was also demonstrated that the aromatic shake-up intensity did not depend on the aromatic substitution degree, [34] thereby suggesting that this loss in intensity can only be attributed to the aromatic ring scission. In the present study, losses of 80 and 70% in the intensity of the $\pi - \pi^*$ shake-up band for the PET films and PET fibres, respectively, were observed following 200 s of plasma treatment (Fig. 4). Thus the XPS data clearly indicate that the ammonia plasma treatment on the PET led to an opening of this polymer's aromatic ring, with a possible scission of the ester groups.

Table 2 HR C1 s spectra curve fitting results of the PET films and fibres before and after plasma treatments of 1 and 200 s

Treatment time	FILM				FIBRE			
	C–C(H)	C–O, C–N N=C	N–C=O N≡C	O–C=O	C–C(H)	C–O, C–N N=C	N–C=O N≡C	O–C=O
Untreated	64.6 ± 0.1	20.3 ± 0.7		15.2 ± 0.8	75.0 ± 1.1	13.8 ± 1.0		11.2 ± 0.4
Plasma 1 s	63.0 ± 2.1	15.0 ± 3.0	7.1 ± 2.1	14.9 ± 1.2	69.6 ± 1.0	13.0 ± 1.9	5.7 ± 1.1	11.7 ± 0.1
Plasma 200 s	63.9 ± 2.6	13.7 ± 0.6	7.3 ± 1.6	15.2 ± 0.9	65.0 ± 1.1	13.2 ± 0.9	6.6 ± 0.8	15.2 ± 0.6

It should also be highlighted that the (C–C, C–H) component of the XPS band located at 285 eV decreased from 75 to 65% of the entire range of this peak for the plasma-treated PET fibres and remained unchanged for the PET films (Table 2). The latter observation, associated to the fact that a greater amount of nitrogen was grafted onto the PET fibres than onto the films (Table 1), may be explained by the grafting of N species (detected at 286.5 eV) on the CH terminal chain groups induced by chain scission during the melt-blowing procedure.

Stability of the Modification

The XPS data recorded after ageing the ammonia plasma-treated samples in water showed that prolonged treatment likely led to polymer chain scissions. These shortened polymer chains did not exhibit good cohesion with the bulk PET and were readily removed/solubilised when exposed to the aqueous environment. As shown in Fig. 5, the 1.6–1.8% of surface amino groups grafted on either the plasma-treated PET films or fibres for 1 s dropped down to 0.3–0.5% after ageing. This observation was even more evident for the PET samples treated for longer periods, as only 0.1% of amino groups remained on the PET films or fibres after ageing. It should be emphasised, however, that the ageing protocol was performed with an ultrasonic bath, thus enabling the removal of most of the loosely

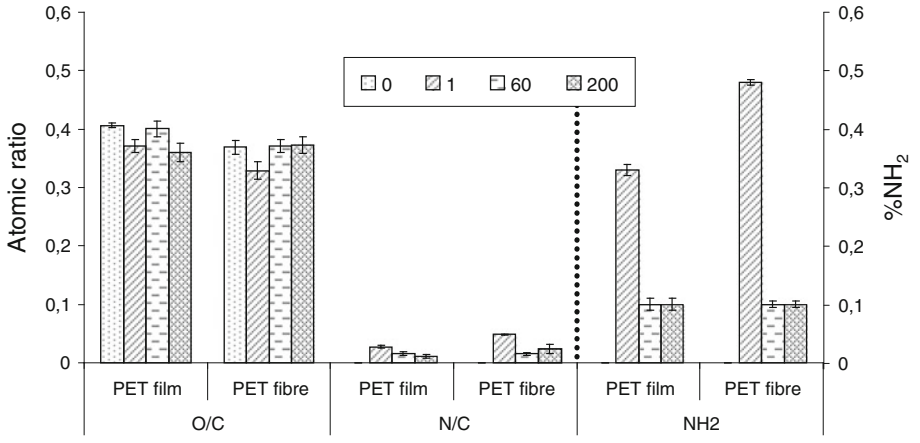

Fig. 5 Ageing effect on the plasma-treated films and fibres characterised by chemical composition (O/C and N/C) and amino concentration (NH_2)

bound polymer fragments. Under these conditions, the 0.3% of amino groups remaining on the aged samples following a plasma treatment of 1 s roughly corresponded to 0.2 amine group per nm^2 and was therefore suitable for molecule surface conjugation.

Despite the fact that there remained N as well as amino groups on the surface, a loss of nitrogen components was also observed (Fig. 5). The N removal may be explained in part by the low molecular weight fragment elimination after washing (5 min in water in an ultrasonic bath). During the NH_3 plasma treatment, as there was formation of imine groups (Table 2, characteristic band in the HR C1s XPS spectra at 286.5 eV) which are readily hydrolyzed in water, some of the initial N grafted post-plasma was therefore reduced.

Surface Topography

The surface topography was scanned tridimensionally by AFM for all of the plasma treatment times, as is shown in Fig. 6 for both the as-treated (a–e) and the aged film samples (f–h), and in Fig. 7 for the fibres. For the aged samples, the 200 s treatment is not

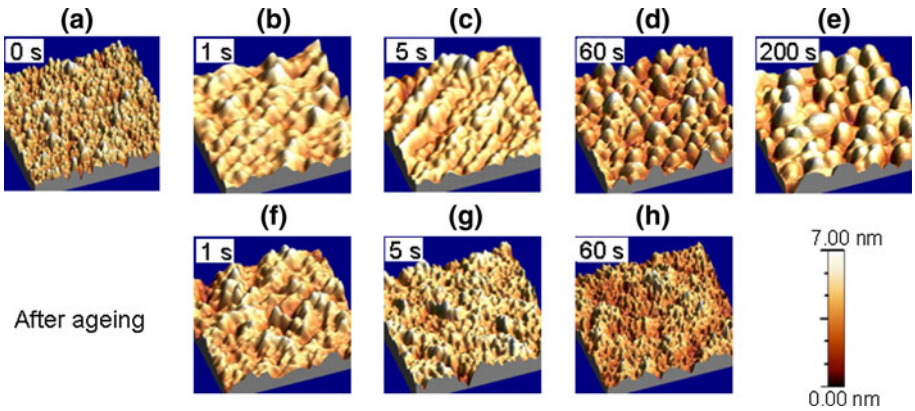

Fig. 6 500 × 500 nm^2 3D AFM images of the untreated and treated PET films after 1, 5, 60, and 200 s: **a–e** before and **f–h** after ageing process

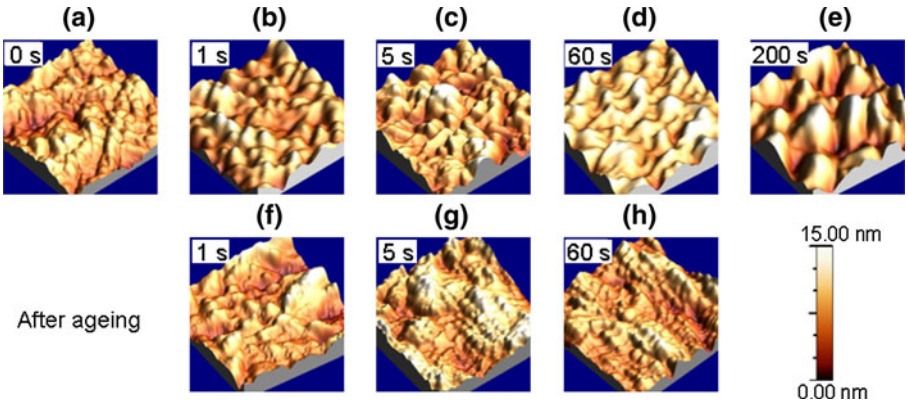

Fig. 7 500 × 500 nm^2 3D AFM images of the untreated and treated PET fibre mats after 1, 5, 60, and 200 s: **a–e** before and **f–h** after ageing process

shown, as it was undistinguishable from the 60 s treatment and was less relevant, as is explained below.

Each topography was composed of round nodules of various sizes, characteristic of agglomeration processes. The fibres also displayed relatively large linear features aligned lengthwise due to their fabrication process (Fig. 7a). Only the films treated for 60 s and aged showed some sharpening indicative of minor pitting effects (Fig. 7h).

Nodule size distribution provided further information as to the physical processes occurring during plasma treatment. Figure 8 shows a typical nodule size distribution obtained from Fig. 6a. The statistical distribution function that best fitted this distribution was the three-parameter log-normal function commonly used to empirically describe different types of agglomeration/fragmentation processes. Including a proportionality constant, it was determined as follows:

$$f[x] = (k/(x - x_0)) \exp[-(1/2)(\ln[(x - x_0/\mu^*)]/\ln \sigma_g)^2$$

where k is the proportionality constant; x_0 is a finite lower limit of x, also called the shift or threshold parameter; μ^* is the scale parameter and the shifted geometrical mean and median (μ^* = geometrical mean − x_0 = median − x_0); and σ_g is the geometrical standard deviation, also called the shape parameter. A $\sigma_g \approx 1$ gives a symmetrical quasi-Gaussian distribution, a $\sigma_g < 1$ gives a negatively skewed asymmetrical distribution, and a $\sigma_g > 1$ gives a positively skewed asymmetrical distribution, as was the case for the ones in this analysis [35–38].

Although the surface areas of the nodules were compiled in the present distributions so as to reduce the possible effects of shape irregularities, and because a product of log-normals is itself lognormal, the diameters or radii were similarly distributed [39, 40]. All of the distributions in the present study displayed a scale parameter close to 2 when fitted with all of the free parameters ($\sigma_g = 1.8 \pm 0.2$), particularly those distributions composed of the greatest number of elements ($\sigma_g = 2.0 \pm 0.2$). This is of great theoretical significance, and will be discussed. It is also mathematically useful. Indeed, in order to reduce the uncertainty on the other parameters, particularly for those distributions composed of the lowest number of elements, σ_g was fixed at 2 which limited the number of adjustable parameters to three, which in turn eased the convergence and decreased uncertainties.

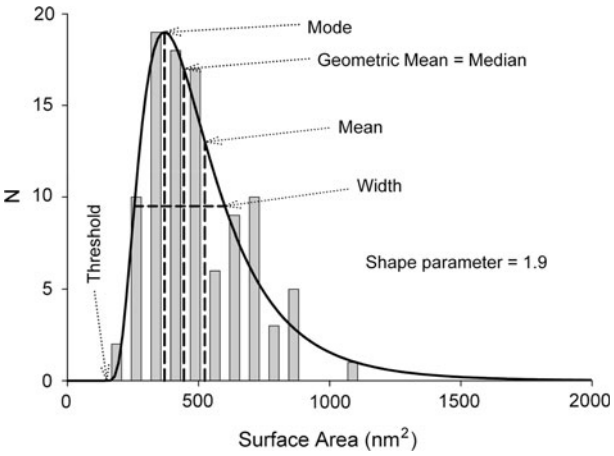

Fig. 8 Nodule size distribution from the AFM images of the untreated PET film (Fig. 6a) with fitted lognormal function

Figure 9a, b show the main distribution parameters of the nodules on the treated films and fibres, respectively. For easier interpretation, they are given in terms of position of maximum (mode) and full width at half maximum (width). Overall, both materials were initially different, as were their fabrication processes, yet both converged towards the same distributions. In addition, a sudden increase followed by a decrease of both parameters was observed in both cases preceding a slower growth. The nodules grew with plasma treatment time but not monotonously. The exact same behaviour was observed quantitatively on both types of aged samples previously treated for up to 5 s (Figs. 9c, d), while longer treatments followed by ageing brought the distribution parameters back to their original values.

The key to understanding these relatively complex effects resides in the shape parameter. Indeed, shape parameter is often quasi-constant for a certain type of agglomeration/fragmentation process and can therefore be considered as a "signature" of the process [40].

Unfortunately, the distribution data presented therein cannot be compared with those of other studies, as no other group has performed such a detailed analysis of PET plasma treatments. Nevertheless, studies on PET plasma treatment all point to an increase of nodule size with treatment duration, in agreement with the present observations [1–3, 14, 41].

Among the well documented agglomeration processes that may be physically related to the present work, only one generally displays typical scale parameters close to 2. During the first steps of evaporated thin film growth of low melting point metals, islands form with distributions displaying a shape parameter between 1.6 and 2.2: a range limited enough to detect unrelated agglomeration processes [39, 42, 43]. In contrast, high melting point metal particles produced under very high temperatures and a thermalised setup are distributed with shape parameters included within the same range [44]. It is interesting to note that droplets in liquid emulsions are also often distributed with a shape parameter close to 2

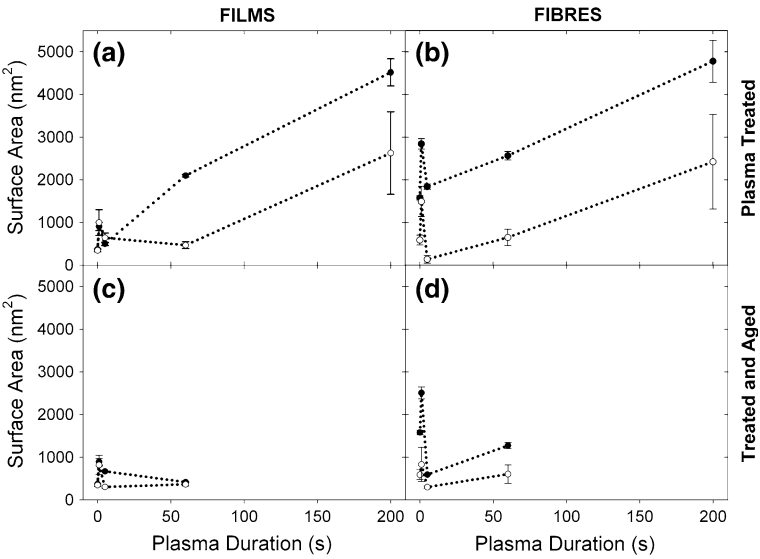

Fig. 9 Main size distribution parameters of the nodules on the treated films and fibres, respectively. Filled circles indicate position of maximum (mode) and empty circles indicate full-width at half-maximum (width)

[45–47]. Incidentally, a link between these two domains has been revealed by studies on the condensation of water vapour on hydrophobic surfaces [48, 49]. All of these experimental findings (except the emulsions) are described qualitatively by the following sequence of events: nucleation and growth of clusters by Brownian diffusion of the incident particles; dynamic liquid-like diffusion and coalescence of the clusters; nucleation and growth of new clusters between the coalesced ones; static coalescence when the clusters are large and close enough to each other.

Inspired by this understanding of the more easily characterised phenomena, the following process can be inferred from the present data:

- The plasma breaks the polymer chains, as shown by XPS (Tables 1, 2, and Fig. 5), and forms mobile fragments.
- These fragments migrate by Brownian motion and tend to agglomerate so as to minimise surface energy; they are hydrophilic in contrast to the underlying hydrophobic material, as evidenced in the contact angle analysis (Fig. 1).
- Small nodules dynamically migrate and coalesce to form large nodules, resulting in a rapid increase of the size distribution parameters.
- The surface exposed by this coalescence then produces new fragments and hence new small nodules leading to the subsequent decrease of the size distribution parameters.
- Once again, the dynamic coalescence increases the size distribution parameters.
- The exposed surface fraction is necessarily smaller, thus new fragment production and the size distribution parameters may continue to oscillate between the data points but with decreasing amplitude.
- Dynamic coalescence proceeds until static coalescence dominates and no remaining fresh material is left exposed.
- The coalesced fragments continue to be further fragmented by the plasma, become increasingly mobile, and enhance the coalescence so much so that they become soluble and are completely washed away by the ageing in water.

This process is deduced from experimental data and logical reasoning from our research as well as that of others aforementioned. Although a theoretical analysis would be beyond the scope of the present paper, some published theoretical work adds significant credence to this hypothesis.

Most of the theoretical models derived to describe/explain log-normal-like distributions from agglomeration processes do not include any notion of threshold parameter, nor anything that may appear or not below it. In our opinion, this is fundamental, thus rendering these models inapplicable to the present case as well as to all the aforementioned experimental studies. A simple shift is easy to construct mathematically yet is physically unjustifiable. Moreover, many of these models are based on the Smoluchowski equation or related ones which appear to be adequate for fully tridimensional systems but are less adequate for partly bidimensional ones, namely, tridimensional aggregates on bidimensional surfaces [50–52].

Computer simulations based on simple rules appear to lead to the most successful models. Results compiled from these simulations can be compared to experimental data and often well approximated by simple analytical formulas. Hence, although the obtained aggregate distributions are never exactly lognormal, they are generally lognormal-like and can be well approximated by the lognormal function, if only for their main part.

Meakin and Family [50–52] investigated the growth of vapour-deposited (low melting point) metal thin films and related phenomena using Monte Carlo simulations and scaling arguments. Among their findings, those relevant and comparable to the present study can

be summarised as follows: The size distributions of the droplets follow a power law decay at small radii due to the continuous nucleation and growth by absorption as well as the distinct "bell-shaped distribution" at large radii caused by coalescence; purely static coalescence would lead to a mean radius varying linearly with time as $\langle R \rangle \sim t$, while dynamic coalescence would lead to $\langle R \rangle \sim t^{<1}$.

Regarding the distributions, very small droplets do indeed appear below the inferior limit of the lognormal-like distribution in some of the afore-mentioned experimental studies. When none are observed, as was the case here, it is difficult to ascertain whether there were in fact none or whether they had merely not been noticed. As is pointed out in detail, [53] the smallest as well as the largest objects are easily missed when such size distributions are measured. This is particularly true in the case of AFM measurements. The Meakin and Family approach can thus be considered compatible with the present case.

The simple radius versus time relations can be quantitatively compared with the present results. When fitted with an equation of the type $y = y0 + ax^b$, the mean surface area versus time (plasma duration) data points, excluding those at 1 s which are part of a spurious effect, leads to the following relations: $\langle \text{surface area} \rangle_{\text{film nodules}} \sim t_{\text{plasma}}^{0.83}$ for the films and $\langle \text{surface area} \rangle_{\text{fibre nodules}} \sim t_{\text{plasma}}^{1.14}$ for the fibres. Considering that the phenomenon is the same in both cases, and by averaging to compensate for the different starting points and remaining oscillatory behaviour, we obtain $\langle \text{surface area} \rangle_{\text{PET nodules}} \sim t_{\text{plasma}}$ and hence $\langle R \rangle_{\text{PET nodules}} \sim t_{\text{plasma}}^{1/2}$. The occurrence of dynamic coalescence is thus supported at least for the samples treated for 60 s or longer for which the relation was the most reliable. Moreover, the exponent of ½ would indicate a negligible connection between the size of the nodules and their diffusion/migration coefficient.

In a study by Beysens et al. [54, 55], numerical simulations were also used with scaling arguments to investigate water vapour condensation on hydrophobic surfaces. The authors focused specifically on the initial steps of the process. Their simulated distributions also displayed a "bell-shaped distribution" which they referred to as a "family" and which became dominant after a certain critical time. Again, these "families" are distinct products of coalescence, have a lognormal-like shape, and are fully scalable over time (i.e., a lognormal fit would have a constant shape parameter). Relations between mean droplet radius and duration are similar to the ones reported by Meakin and Family, except that they concern only the "family" droplets after the critical time, with static coalescence leading to $\langle R \rangle \sim t$ and dynamic coalescence leading to $\langle R \rangle \sim t^{0.48}$. This particular relation corresponds precisely to the present study and further supports the occurrence of dynamic coalescence, as this coalescence was indeed dominant for a plasma treatment shorter than 60 s, and the "universal" lognormal distribution with a constant shape parameter confirms that dynamic coalescence was significant on all of the samples, including the virgin ones.

Mobile fragments were therefore produced during both material fabrication processes. The nodules were however much larger on the virgin fibres than on the virgin films (Fig. 9a, b), indicating that coalescence and hence fragmentation were already much more advanced on the melt-blown fibres. This confirms the XPS results showing that shorter, more damaged polymer chains formed on the surface of the PET fibres.

The resulting data therefore clearly demonstrate that the subsequent surface chemistry of the plasma-treated PET depended on the polymer forming process, as it influenced the initial formation mechanism of the surface mobile fragments. This important observation is often underestimated, as most plasma surface modification studies make no connection between the initial state of the polymer surface and its plasma-treated counterpart. Moreover, most studies conclude matter-of-factly that etching is responsible for nodule

formation and the increased roughness, a conclusion that clearly contradicts the present analysis.

The Monte Carlo statistical model of R. Hrach et al. simulates the early stages of evaporated metal film formation [56–58]. It has culminated into a very fundamental model where atomistic processes are simulated by molecular dynamics and larger-scale events are simulated by Monte Carlo kinetics [59]. The latest published size distributions correspond very well qualitatively to the distributions presented in our study. This promising model is unfortunately poorly documented and no quantitative comparison can be made with it. Nevertheless, some information may be gathered from the initial assumptions that lead to the most successful simulations. It would thus appear that particles are much more strongly attracted by the clusters than by the substrate, that the coalescence phenomenon is, in fact, both liquid-like and very rapid, compared to all other processes, and that the migration of clusters does occur but with a probability inversely proportional to size.

This assumption appears to contradict the one emanating from the Meakin and Family approach showing an independence of migration coefficient on size and concerning only the samples treated for 60 s or longer. The heavy, time-consuming computer simulations of R. Hrach et al. are necessarily limited in virtual time and are thus more applicable to samples treated for short durations. The continuous fragmentation of the fragments that are coalesced into nodules would effectively reverse the usual diffusion versus size relationship, thereby rendering the longer-treated, larger nodules more mobile compared to the less-treated/smaller ones. The solubility of these large nodules is thus readily explained.

Finally, it is noteworthy that Strobel et al. have reached similar conclusions about the similar topography of corona discharge-oxidized polypropylene using well-supported but different, comparative, qualitative reasoning [60].

Conclusions

Our findings highlight the effect of the PET forming process on the surface chemistry of this polymer upon plasma surface modification. To this end, commercially available PET films and melt-blown PET fibres were investigated. XPS experiments on these samples revealed that the melt-blowing process led to PET chain scissions, which mainly affected the polymer's aromatic ring. On the other hand, radiofrequency low pressure plasma treatment in ammonia allowed for the incorporation of amino functionalities on both the PET films and melt-blown fibres, with the highest amino group surface concentration obtained for a very short treatment time (1 s). Surface treatments for longer periods led to chain scissions which occurred on either the aromatic rings or the ester groups. These small polymer chain fragments tended to aggregate, as evidenced by AFM. In addition, ageing the plasma-treated PET samples in water revealed that this polymer chain fragmentation led to a loss of cohesion between the coalesced polymer fragments and the underlying material, as indicated by the restoration of surface features characteristic of the untreated samples. Finally, our data also clearly show that the untreated melt-blown PET fibres already exhibited surface features similar to those observed on the PET films following 1–5 s of plasma treatment. This observation confirms that the process used to produce the polymer fibres induced surface damages resembling those observed upon plasma treatment. In this context, the polymer forming process must be taken into account when performing surface plasma treatments, as it somewhat defines the initial state of the polymer's interfacial and cohesive properties.

Acknowledgments The authors wish to thank the National Science and Engineering Research Council (NSERC) and the Centre québécois sur les matériaux fonctionnels (CQMF) for their financial support. They also acknowledge the contribution of Dr. Abdellah Ajji and Mr. Jacques Dufour of NRC-IMI in the fabrication of the PET fibre mats, as well as that of Maude Larouche of Université Laval in the AFM image analyses.

References

1. Inagaki N, Narushim K, Tuchida N, Miyazaki K (2004) J Polym Sci Part B Polym Phys 42:3727–3740
2. Navaneetha Pandiyaraj K, Selvarajan V, Deshmukh RR, Gao C (2008) Vacuum 83:332–339
3. Yang L, Chen J, Guo Y, Zhang Z (2009) Appl Surf Sci 255:4446–4451
4. Vesel A, Junkar I, Cvelbar U, Kovac J, Mozetic M (2008) Surf Interf Anal 40:1444–1453
5. Janca J, Stahel P, Buchta J, Subedi D, Krcma F, Pryckova J (2001) Plasmas Polym 6:15–26
6. Wang GJ, Liu YW, Guo YJ, Zhang ZX, Xu MX, Yang ZX (2007) Surf Coat Technol 201:6565–6568
7. Öktem T, Ayhan H, Seventekin N, Piskin E (1999) J Soc Dyers Colour 115:274–279
8. Wang CX, Liu Y, Xu HL, Ren Y, Qiu YP (2008) Appl Surf Sci 254:2499–2505
9. François S, Chakfé N, Durand B, Laroche G (2009) Acta Biomater 5:2418–2428
10. Chlupac J, Filova E, Bacakova L (2009) Physiol Res 58:S119–S139
11. Esquivel CO, William Blaisdell F (1986) J Surg Res 41:1–15
12. Chakfé N, Bizonne SC, Beaufigeau M, Urban E, Cardon A, Doillon C, Le Magnen J-F, Durand B, Kretz J-G (1999) Ann Vasc Surg 13:509–523
13. Greenwald SE, Berry CL (2000) J Pathol 190:292–299
14. Navaneetha Pandiyaraj K, Selvarajan V, Deshmukh RR, Bousmina M (2008) Surf Coat Technol 202: 4218–4226
15. Narushima K, Yamashita N, Fukuoka M, Inagaki N, Isono Y, Rafiqul Islam M (2007) Jpn J Appl Phys 46:4238–4245
16. Narushima K, Yamashita N, Isono Y, Islam MR, Takeuchi M (2008) Jpn J Appl Phys 47:3603–3605
17. Inagaki N, Narushima K, Lim SK (2003) J Appl Polym Sci 89:96–103
18. Aflori M, Drobotă M, Ţîmpu D, Bărboiu V (2007) Amine functionality of poly(ethylene terepthalate) films surfaces induced by chemical and RF plasma treatments" 28th ICPIG, July 15–20, 2007. Prague, Czech Republic, pp 727–730.
19. Fang Z, Lin J, Yang H, Qiu Y, Kuffel E (2009) IEEE Trans Plasma Sci 37:659–667
20. Girardeaux C, Zammatteo N, Art M, Gillon B, Pireaux J, Caudano R (1996) Plasmas Polym 1:327–346
21. Schröder K, Meyer-Plath A, Keller D, Besch W, Babucke G, Ohl A (2001) Contrib Plasma Phys 41:562–572
22. López-Santos C, Yubero F, Cotrino J, González-Elipe AR (2010) Appl Mater Interf 2:980–990
23. Grace J, Gerenser L (2003) J Dispers Sci Technol 24:305
24. Pu FR, Williams RL, Markkula TK, Hunt JA (2002) Biomaterials 23:2411–2428
25. Sipehia R, Martucci G, Barbarosie M, Wu C (1993) Biomat Art Cells Immobil Biotechnol 21:455–468
26. Ramires PA, Mirenghi L, Romano AR, Palumbo F, Nicolardi G (2000) J Biomed Mater Res 51:535–539
27. Goddard JM, Hotchkiss JH (2007) Prog Polym Sci 32:698–725
28. Chevallier P, Janvier R, Mantovani D, Laroche G (2005) Macromol Biosci 5:829–839
29. Junkar I, Cvelbar U, Vesel A, Hauptman N, Mozetič M (2009) Plasma Process Polym 6:667–675
30. Moreno MJ, Ajji A, Mohebbi-Kalhori D, Rukhlova M, Hadjizadeh A, Bureau MN (2011) J Biomed Mater Res B Appl Biomater 97:201–214
31. Chevallier P, Castonguay M, Turgeon S, Dubrulle N, Mantovani D, McBreen PH, Wittmann J-C, Laroche G (2001) J Phys Chem B 105:12490–12497
32. Gauvreau V, Chevallier P, Vallieres K, Petitclerc E, Gaudreault RC, Laroche G (2004) Bioconjugate Chem 15:1146–1156
33. Mantovani D, Castonguay M, Pageau JF, Fiset M, Laroche G (1999) Plasmas Polym 4:207–228
34. Beamson G, Briggs D (1992) High resolution XPS of organic polymers: the Scienta ESCA300 database. Wiley, Chichester
35. Balakrishnan N, Chen WWS (1999) Chen handbook of tables for order statistics from lognormal distributions with applications. Kluwer, Amsterdam
36. Crow EL, Shimizu K (1988) Lognormal distributions: theory and applications. New York: Dekker, M.
37. Gutiérrez R, Gutiérrez-Sánchez R, Nafidi A, Ramos E (2009) J Stat Comput Sim 79:25–38
38. Wagner LE, Ding D (1994) Trans ASAE 37:815–821

39. Granqvist CG, Buhrman RA (1976) J Appl Phys 47:2200–2219
40. Limpert E, Stahel WA, Abbt M (2001) Bioscience 51:341–352
41. Gupta B, Hilborn J, Hollenstein C, Plummer CJG, Houriet R, Xanthopoulos N (2000) J Appl Polym Sci 78:1083–1091
42. Regnier S, Renou A, Gillet M (1993) Mater Sci Eng B Solid B18:169–177
43. Sugawara A, Nakamura Y, Nittono O (1990) J Cryst Growth 99:583–587
44. Udaka M, Kawasaki K, Yamazaki T, Umemoto M, Okane I (1994) J Jpn Inst Metals 58:683–690
45. Rajagopal ES (1959) Proc Indian Acad Sci A 49:333–339
46. Shaughnessy RJ, Byeseda JJ, Sylvester ND (1983) Ind Eng Chem Prod Res Dev 22:473–478
47. Van Dalen G (2002) J Microc 208:116–133
48. Beysens D, Knobler CM, Schaffar H (1990) Phys Rev B 41:9814–9818
49. Zuo JM, Li BQ (2002) Phys Rev Lett 88:255502/1–255502/4
50. Family F, Meakin P (1988) Phys Rev Lett 61:428–431
51. Meakin P (1990) Phys A 165:1–18
52. Meakin P, Family F (1989) J Phys A Math Gen 22:L225–L230
53. Proussevitch AA, Sahagian DL, Tsentalovich EP (2007) J Volcanol Geoth Res 164:95–111
54. Fritter D, Knobler CM, Beysens D (1991) Phys Rev A 43:2858–2869
55. Steyer A, Guenoun P, Beysens D, Knobler CM (1991) Phys Rev A 44:8271–8277
56. Boldys J, Hrach R (1999) Superficies y Vacio 9:32–36
57. Hrach R (1990) Int J Electron 69:55–64
58. Hraqch R (1992) Vacuum 43:705–708
59. Hrach R, Simek J, Kostern M (2002) Vacuum 67:229–233
60. Strobel M, Jones V, Lyons CS, Ulsh M, Kushner MJ, Dorai R, Branch MC (2003) Plasmas Polym 8:61–95